J. Fluid Mech. (2017), *vol.* 821, *pp.* 624–646.
doi:10.1017/jfm.2017.204

Laminar hypersonic leading edge separation – a numerical study

Amna Khraibut[1,†], S. L. Gai[1], L. M. Brown[1] and A. J. Neely[1]

[1]School of Engineering and Information Technology, Northcott Drive, Canberra ACT 2612, Australia

(Received 1 June 2016; revised 26 March 2017; accepted 27 March 2017;
first published online 25 May 2017)

This paper describes laminar hypersonic leading edge separation. Such a configuration of separated flow was originally studied by Chapman *et al.* (*NACA Tech. Rep.* 1356, 1958) at supersonic Mach numbers as it is particularly amenable to theoretical analysis and assumes no pre-existing boundary layer. It can be considered as a limiting case of much studied generic configurations such as separation at a compression corner and separated flow behind a base. A numerical investigation is described using a compressible Navier–Stokes solver assuming perfect gas air, no slip boundary condition and a non-catalytic surface. A moderate enthalpy flow of 3.1×10^6 J kg^{-1} with a unit Reynolds number of 1.34×10^6 m^{-1} and a Mach number of 9.66 was considered. The resulting separated flow is analysed in the context of viscous–inviscid interaction and interpreted in terms of 'triple-deck' concepts. Particular emphasis is given to wall temperature effects. The effects of strong to moderate wall cooling on flow in the separated region as well as on processes of separation, reattachment and separation length, are highlighted. The numerical simulations have also shown the existence of a secondary eddy embedded within the primary recirculation region, with its size, shape and position, being strongly affected by the wall temperature.

Key words: boundary layer separation, computational methods, high-speed flow

1. Introduction

With the advent of supersonic and transonic aircraft, a particular type of flow separation that results from a strong interaction between shock waves and boundary layers attracted intense attention of researchers. Such shock wave/boundary layer interactions (SBLI) occur on many parts of aircraft such as wings, control surfaces, intakes etc. and can be quite detrimental to the performance of the aircraft. Many theoretical, numerical and experimental investigations have since been conducted to fully understand the phenomenon of SBLI for more than half a century. Especially well-known studies, which have contributed to our theoretical understanding of this problem, are by Lighthill (1953), Gadd (1957), Chapman, Kuehn & Larson (1958), Brown & Stewartson (1969), Neiland (1969), Stewartson & Williams (1969), Messiter (1970), Neiland (1970) and Neiland (1973). The major advance in understanding laminar SBLI and separation was made by Brown & Stewartson (1969), Neiland (1969), Stewartson & Williams (1969) and Neiland (1970). They developed a rigorous

† Email address for correspondence: amna.khraibut@student.adfa.edu.au

theory based on an asymptotic approach to the full Navier–Stokes equations in which the interacting boundary layer is divided into three layers (the 'triple deck'); the viscous sublayer adjacent to the wall, the largely inviscid rotational flow in the main or middle layer and the outer inviscid irrotational (potential) flow. The triple-deck theory enables the effects of pressure perturbations caused by the shock wave on the boundary layer in each of these layers to be taken into account then by appropriately matching the boundary conditions of each layer, it yields a self-consistent set of equations which can be solved either numerically or analytically. The solutions then yield the characteristic parameters of laminar SBLI, such as separation, pressure plateau, peak pressures and the upstream influence. More elaborate interpretations of the subtleties of the separation and reattachment processes and the characteristics of laminar SBLI have been given by Smith (1986), Smith & Khorrami (1991) and Korolev, Gajjar & Ruban (2002). Although the triple-deck theory is an asymptotic theory strictly valid only for very high Reynolds number flows, it has been shown to give reasonable estimates of parameters even for the moderate Reynolds number flows encountered in many experimental situations (Rizzetta, Burggraf & Jenson 1978; Burggraf *et al.* 1979; Katzer 1989).

Hypersonic SBLIs have attracted the attention of researchers since the seventies and eighties with the arrival of the age of the space shuttle and other space planes flying at hypersonic speeds. Major contributions to hypersonic SBLI have been due to Neiland (1973), Brown, Stewartson & Williams (1975), Rizzetta *et al.* (1978), Gajjar & Smith (1983) and Smith & Khorrami (1991). Thermal effects in hypersonic boundary layers, particularly wall cooling and its effects on SBLI, have also been investigated in recent years and analysed in terms of triple-deck theory (Brown, Cheng & Lee 1990; Seddougui, Bowles & Smith 1991; Kerimbekov, Ruban & Walker 1994; Cassel, Ruban & Walker 1995, 1996; Neiland, Sokolov & Shvedchenko 2009; Shvedchenko 2009). Moreover, Khorrami & Smith (1994) presented complete solutions to the hypersonic interactive boundary layer for a semi-infinite plate and thin airfoils, which included both the effects of wall enthalpy and the viscous interaction parameter on the upstream influence. They also looked at the effects of velocity slip and temperature jump. A comprehensive account of hypersonic SBLI and separation and application of triple-deck theory has been given in reviews by Stewartson (1974), Smith (1986), Sychev *et al.* (1998) and Neiland *et al.* (2008). An analytical solution for reattachment flow has been obtained in Smith (1988).

Herein, we present an investigation pertaining to hypersonic viscous interaction and separation using the so-called leading edge separation configuration. This particular configuration was first considered and investigated by Chapman *et al.* (1958) at supersonic Mach numbers and moderate to high Reynolds numbers. The hypersonic SBLI on such a configuration does not appear to have been investigated in detail so far and was the motivation for the present study. Wall temperature effects on this type of separation are also considered.

2. Model geometry and flow conditions

In order to understand the basic characteristics of hypersonic flow separation, we consider a leading edge separation configuration. Chapman *et al.* (1958), as mentioned earlier, first used this configuration as it is particularly well suited for theoretical analysis, and the authors used it as such to develop their isentropic recompression theory to predict base pressures behind bluff bodies. Their rationale in using this geometry was that it precludes the effects of a pre-existing boundary layer and hence

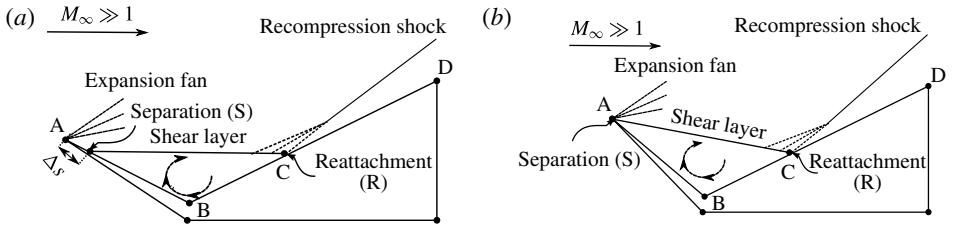

FIGURE 1. Evolution of separation in compression corners: (*a*) finite separation length; (*b*) leading edge separation ($\Delta s \to 0$). Δs is the distance from the leading edge to separation.

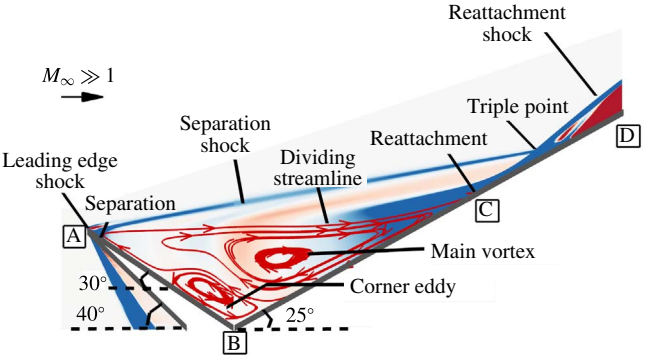

FIGURE 2. Schematic of flow structure of hypersonic leading edge separation (baseline case) and geometry.

made it easy to use laminar mixing layer theory. Chapman *et al.* (1958) point out further that, in fact, the leading edge separation arrangement can be considered as a limiting case of both separation behind a base and compression corner, wherein the distance from the leading edge to separation point Δs reduces to zero (figure 1). Later, Stewartson (1964) and Brown & Stewartson (1969) mentioned leading edge separation without taking it further except to say that it is worth exploring the assumptions, made by Chapman *et al.* (1958) from a more rigorous standpoint. The investigation of Chapman *et al.* (1958) was restricted to low to moderate supersonic Mach numbers and moderate to high Reynolds numbers. It is, therefore, of sufficient interest to examine the properties of such a separation under viscous flow conditions, when the Mach numbers are high and Reynolds numbers are low, as encountered during hypersonic flight at high altitude such as re-entry. The present investigation is restricted to two-dimensional steady hypersonic laminar separated flows.

Figure 2 shows a schematic of the leading edge configuration used in the numerical study with main flow features. Here, the corner angle at *B* is selected so that it is large enough to ensure separation at (or very near) the sharp leading edge at *A*. This configuration is equivalent to a compression corner of deflection angle 55°, whose upstream plate *AB* has been tilted around the corner at a large positive incidence angle of 30°, instead of being parallel to the free stream (see Chapman *et al.* 1958). Ideally, after expansion, a thin shear layer, in which the velocity varies from zero to the local external stream value, emanates from *A* and reattaches at *C*. A large recirculation region is thus formed and bounded by *ABC* in which a shear layer *AC* separates

p_o (Pa)	h_o (J kg^{-1})	T_o (K)			
11.3×10^6	3.1×10^6	3150			
M_∞	Re_∞ (m^{-1})	U_∞ (m s^{-1})	p_∞ (Pa)	T_∞ (K)	ρ_∞ (kg m^{-3})
9.66	1.34×10^6	2503	288.9	165	0.006

TABLE 1. Nozzle reservoir and free-stream conditions (Park *et al.* 2010).

it from the outer inviscid flow. Under hypersonic conditions, due to strong viscous effects at the leading edge, the expansion is preceded by a weak leading edge shock wave.

Table 1 shows the flow conditions used in numerical simulations. These flow conditions were previously obtained from a free-piston-driven shock tunnel as per Park, Gai & Neely (2010). In table 1, h, T, p and Re, denote the specific enthalpy, temperature, pressure, density and Reynolds number, respectively, whereas subscripts 'o' and ∞ refer to the reservoir and free-stream conditions, respectively. To investigate the effects of wall temperature T_w, three isothermal walls of 165, 300 and 800 K, and an adiabatic wall have been considered. The selection of wall temperatures essentially represent the free-stream temperature, a baseline, an intermediate and a limiting case of an adiabatic wall. These wall temperatures correspond, respectively, to wall to stagnation temperature ratios s_w of 0.05, 0.1, 0.25 and 0.88, and reflect a range varying from strong cooling to no heat flux into the wall.

3. Theoretical considerations

3.1. *The triple-deck structure of a compressible boundary layer*

Figure 3 shows a basic triple-deck structure centred at a compression corner with a typical separation velocity profile as shown by the red dashed line. Here, the x and y coordinates express the streamwise and transverse directions, respectively, and $\epsilon = Re^{-1/8}$ is the controlling parameter in the triple-deck theory, where Re is a characteristic Reynolds number, assumed asymptotically large, based on the free stream and length L_e. The boundary layer profile in the interaction region is characterised in terms of a main, upper and lower deck, and each is assigned a thickness in terms ϵ. The main deck in which the fluid is largely inviscid and rotational is of the order ϵ^4. The upper deck, where the fluid is inviscid and irrotational, is of the order ϵ^3. Finally, the lower deck, where viscous effects are dominant, is of the order ϵ^5. The pressure (Δp) and velocity (Δu) perturbations are assumed to be of the order ϵ^2 and ϵ, respectively. The pressure and velocity perturbations are assumed to spread over a streamwise distance (Δx) of the scale ϵ^3 called the interaction region. The scaled value of the corner angle α is of the order ϵ^2, and the normalised distance from the leading edge to the corner is 1.

Analyses of laminar SBLI, based on triple-deck theory were given by Neiland (1969), Stewartson & Williams (1969) and Neiland (1970). The basis of this theory is that the whole interaction process is controlled by the lower deck, the equations of which are essentially those of the incompressible boundary layer. Neiland (1970), Neiland (1973), Stewartson (1975), Rizzetta *et al.* (1978), Gajjar & Smith (1983),

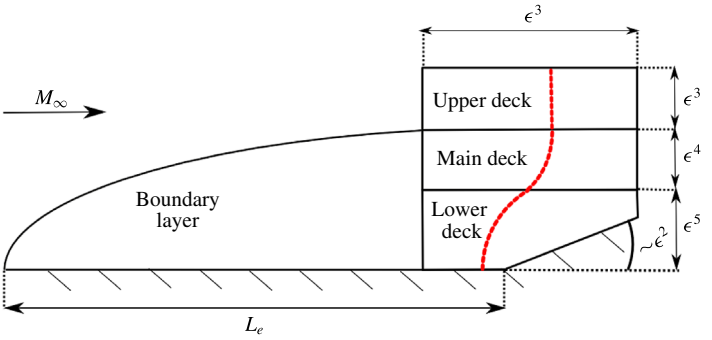

FIGURE 3. (Colour online) Triple-deck structure in corner flows. Dashed line is a separated velocity profile.

Smith & Khorrami (1991) and Sychev *et al.* (1998) have since shown that the triple-deck approach, by using appropriate boundary conditions, is equally valid in hypersonic interactive boundary layers with (or without) wall cooling. In terms of scaled variables (Stewartson & Williams 1969; Rizzetta *et al.* 1978; Gajjar & Smith 1983), the governing equations for a steady two-dimensional flow are,

$$\frac{\partial U}{\partial X}+\frac{\partial V}{Y}=0, \tag{3.1}$$

$$U\frac{\partial U}{\partial X}+V\frac{\partial U}{\partial Y}=-\frac{\partial P}{\partial X}+\frac{\partial^2 U}{\partial Y^2}, \tag{3.2}$$

$$\frac{\partial P}{\partial Y}=0, \tag{3.3}$$

where U and V are the streamwise and transverse velocities, respectively, X is the streamwise direction, Y is the transverse direction and P is the pressure. The governing boundary condition are as $Y\to\infty$, $U\to Y+A(X)$, at the wall, $U=V=0$, and as $X\to\infty$, $(U, V, P'A)\to(Y, 0, 0, 0)$, where the prime notation indicates the derivative in the streamwise direction. Here, $A(X)$ is an arbitrary function describing the change in displacement thickness in a self-induced separation.

For a supersonic outer flow, the pressure perturbation in P is obtained by invoking the Ackeret relation so that $P(X)=-A'(X)$. For hypersonic flow, the pressure–displacement relation is obtained through the tangent-wedge approximation as was first proposed by Neiland (1970) and discussed in Stewartson (1975), Gajjar & Smith (1983) and Smith & Khorrami (1991). A more generalised expression, which includes the effects of wall cooling is given by Brown *et al.* (1990) in the form,

$$-\frac{\mathrm{d}A}{\mathrm{d}X}=\frac{\mathrm{d}P}{\mathrm{d}X}+\frac{1}{\sigma}P(X), \tag{3.4}$$

where σ is a parameter, which includes the effects of both hypersonic viscous interaction parameter $\bar{\chi}$ and wall cooling. σ is given in Brown *et al.* (1990) as,

$$\sigma=\left(\frac{s_w^*}{s_w}\right)^{4\omega+2}, \tag{3.5}$$

where s_w is the wall temperature to stagnation temperature ratio T_w/T_o, and s_w^* is the critical wall temperature ratio defined in Cheng (1993) as,

$$s_w^* \sim \frac{T^*}{T_o} \sim \left[\lambda^5 \gamma^{-1/2} \left(\frac{2}{\gamma - 1}\right)^2 \bar{\chi}\right]^{1/(4\omega+2)}, \tag{3.6}$$

where λ is a normalised undisturbed wall shear, γ is the specific heat ratio of air and $\bar{\chi}$ is the hypersonic viscous interaction parameter evaluated at the corner. ω is the viscosity index, which ranges from 0.5 to 1 and for strong wall cooling, the lower limit is usually taken (see Brown *et al.* 1990). The term $2/(\gamma - 1)$ is called the Newtonian factor, and when $(\gamma - 1)/2 \ll 1$ and $M \gg 1$, the use of tangent-wedge approximation of Neiland (1970) is justified. If the boundary layer upstream of the interaction is a fully developed Blasius profile, then with $\gamma = 1.4$ and $\lambda = 0.332$, we get,

$$\sigma \sim 0.085 \bar{\chi} s_w^{-4}, \tag{3.7}$$

which shows that σ is proportional to the hypersonic viscous interaction parameter, but more importantly, rapidly increases with decreasing wall temperature.

The hypersonic viscous interaction parameter usually defined as $\bar{\chi} = M^3(C/Re)^{1/2}$ (Hayes & Probstein 1959) is based on the distance from the leading edge A to the corner B. Various authors, for example, Rizzetta *et al.* (1978), Smith & Khorrami (1991), Korolev *et al.* (2002), Neiland *et al.* (2009) and Shvedchenko (2009) have used the distance from the leading edge to the compression corner as the characteristic dimension of the problem. Brown *et al.* (1990), on the other hand, have taken the distance from the plate leading edge to the beginning of interaction as the characteristic length, while Katzer (1989) used the distance from the leading edge to the point of shockwave impingement on a plate as the characteristic dimension. Herein, to be consistent, we use the distance from the leading edge to the corner (length AB in figure 2) as the characteristic dimension for the evaluation of $\bar{\chi}$. In the expression for $\bar{\chi}$, C is the Chapman–Rubesin constant.

It has been shown by Gajjar & Smith (1983) that in the special case of $\sigma \to \infty$, the expression $P(X) = -A(X)$ reduces to simple hypersonic free interaction that exhibits power-law growth of pressure with X. Brown *et al.* (1990) point out that for large (but finite) value of σ, a plateau in P (for large X) is possible. Their numerical calculations, however, did not indicate a plateau for $\sigma > 10$. Gajjar & Smith (1983) also showed that $P(X) = -A(X)$ can equally describe a supercritical hydraulic jump in a shallow liquid layer down an inclined plane.

A somewhat different approach was taken by Neiland (1973) and his associates (see for example, Kerimbekov *et al.* 1994, Cassel *et al.* 1995 and Cassel *et al.* 1996). Kerimbekov *et al.* (1994) describes the interactive equation as,

$$-\frac{\mathrm{d}A}{\mathrm{d}X} = P(X) - N^{3/4}\frac{\mathrm{d}P}{\mathrm{d}X}, \tag{3.8}$$

where N is the Nieland number (Cassel *et al.* 1996), defined as,

$$N = S|\mathcal{L}|^{4/3}. \tag{3.9}$$

When $N \ll 1$, the flow is subcritical (wall cooling), supercritical (wall heating) when $N \gg 1$, and transcritical (approaching adiabatic) when $N \sim O(1)$. This is equivalent to $s_w^*/s_w \ll 1$, $s_w^*/s_w \gg 1$ and $s_w^*/sw \sim O(1)$, respectively, in Brown *et al.* (1990) terminology.

Numerical calculations on a compression corner in hypersonic flow carried out by Cassel *et al.* (1996), based on Neiland's approach, show that a pressure plateau exists, for all values of N, after separation and downstream of the corner, in contrast to Brown *et al.* (1990). They, also, found that increasing N (equivalently σ) causes the separation point to move towards the corner. The separation region extent Δx, as shown by Neiland *et al.* (2009), also decreases with decreasing s_w (increasing N), since,

$$\frac{\Delta x}{L_e} = \left(\frac{\Delta p}{p}\right) s_w^{(2\omega+1)/2}. \tag{3.10}$$

These hypersonic triple-deck theories are based on certain important assumptions. Firstly, they are asymptotic theories valid at high Reynolds numbers, and generally assume $\bar{\chi} \sim O(1)$ or less. The Newtonian approximation that $(\gamma - 1)/2 \ll 1$, and $M \gg 1$ is, in general, required to hold. It is assumed, therein, that prior to the interaction with a sudden pressure disturbance (typically, a compression corner or an incident shock wave), the boundary layer is fully developed, and the separation process resulting from the interaction is 'free' and spontaneous (Chapman *et al.* 1958; Neiland 1969; Stewartson & Williams 1969). Such interaction is not influenced by downstream conditions and is independent of the agency provoking separation. Finally, it is assumed that the interaction region is small ($\sim Re^{-3/8}$), and separation is small enough to be contained within it. In recent years, however, there have been attempts to study large-scale separations within the general framework of hypersonic triple-deck theory by Neiland (1973), Brown *et al.* (1975), Brown *et al.* (1990), Smith & Khorrami (1991), Sychev *et al.* (1998), Neiland *et al.* (2009) and Shvedchenko (2009), with some success.

In what follows, the leading edge separation problem will be investigated and analysed in the context of hypersonic triple-deck framework and large separated regions.

4. Computational approach

4.1. *General description of numerical solver and assumptions*

The numerical simulations were carried out using the compressible Navier–Stokes solver, US3D. The code was developed by Candler and his associates at the University of Minnesota (Nompelis & Candler 2014; Candler *et al.* 2015), and is capable of modelling both perfect and real gases. The code has been validated for simple and complex geometries (Drayna, Nompelis & Candler 2006; Holden *et al.* 2013; Candler, Subbareddy & Brock 2014) at hypersonic speeds. In the real gas simulations, the code solves the conservation equations by using law of mass action for chemical species, whereas reaction rates are given in the Arrhenius form. Equilibrium constants are determined by using the NASA Lewis CEA database. The code uses the two-temperature kinetic model of Park (1993), but in this instance, a combined translational–rotational and vibrational temperature is used for the perfect gas. The energy exchange is based on the Landau–Teller equation, and vibrational relaxation times are based on Millikan & White (1963) empirical correlations.

The code uses a finite volume method to solve three-dimensional Navier–Stokes equations, and is capable of both steady-state and transient solutions. The steady-state solution is obtained by using the modified Steger–Warming flux vector splitting method (Candler *et al.* 2015), and monotone-upstream-conservative-limited scheme (Van Leer 1979) to obtain higher-order spatial accuracy. To maintain low dissipation,

Index (k)	Description	n (Million)
1	Very fine	>3
2	Fine	2–3
3	Medium	∼1
4	Coarse	<1

TABLE 2. Description of grids used in the simulations where n is the number of cells.

as it is necessary in hypersonic simulations, the code uses the Osher limiter by default (Nompelis & Candler 2014). To achieve faster convergence, the code uses the data-parallel-line-relaxation approach (Wright, Candler & Bose 1998), and in the present study, the implicit scheme is used.

The simulations assumed perfect gas air with constant specific heat ratio γ of 1.4, and transport properties were evaluated using Wilke's mixing rule (Wilke 1950; Blottner, Johnson & Ellis 1971). For the flow conditions given in table 1, air is assumed to be a continuum, laminar and without slip or temperature jump at the wall. Further, the wall is assumed to be non-catalytic.

4.2. *Grid generation and boundary conditions*

In the present study, structured grids were generated for all wall temperatures to carry out a grid independence study. Table 2 describes these grids based on their number of cells n and overall quality. Here, 'coarse' is used to describe grids with $n < 1$ million, 'medium', for grids with $n \sim 1$ million, 'fine', for grids with n between 2 and 3 million and finally, 'very fine', for grids with n much greater than 3 million.

In figure 4, the coarse grid of the baseline case ($s_w = 0.1$) is shown. The blue line defines the computational domain boundaries. In the solver, the boundary conditions were the same for all the grids used, except for minor differences in the specification of wall temperature. The domain boundaries are labelled in figure 4 and correspond to the appropriate boundary condition. Edges 1 and 2 are the supersonic velocity inlets, edges 3 and 6 are the outflow, edges 4–6 are the walls specified either as isothermal walls as in $s_w = 0.05$, 0.1 and 0.25, or adiabatic as in $s_w = 0.88$. Given the critical flow features near the leading edge, corner and reattachment, cells in these regions were clustered as necessary. To ensure a good flow resolution near the walls, a constant first cell height Δs_w of 1 μm was used for all grids. A Courant–Friedrichs–Lewy number larger than 200 was possible for most simulations. Starting from the coarse grid, grid refinement was achieved by successively increasing the number of cells n by a factor of ∼2.1 on average.

4.3. *Convergence studies*

To verify the accuracy of the numerical solver, grid solutions were checked for both iterative and overall grid convergence. Iterative convergence is typically done by monitoring residuals as reported by the solver, and the solution is said to be iteratively converged if the residuals drop by at least 5 orders of magnitude. Overall grid convergence is determined by using an appropriate grid error analysis method. Additional convergence checks were made by checking changes in surface parameters as they settle to their steady-state values with successive iterations. In the present

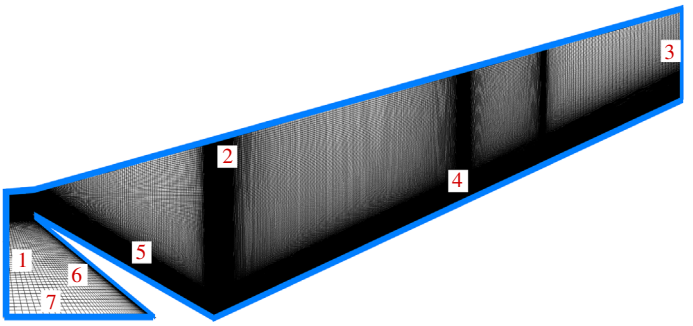

FIGURE 4. (Colour online) Baseline grid. The blue line defines the computational domain boundaries. Numbers seen on the edges refer to the boundary conditions. Edge 5 is 20 mm for all grids. To accommodate the increase in separation length due to wall temperature, edge 4 was extended to 80 mm and 100 mm for $s_w = 0.25$ and $s_w = 0.88$, respectively.

case, the parameters of interest are the shear stress τ_w^*, pressure p_w^* and heat flux q_w^*. Superscript '*' refers to normalised quantities of the dimensional shear stress and surface pressure by the dynamic pressure $0.5\rho U_\infty^2$, dimensional heat flux by $0.5\rho U_\infty^3$ and s^* is the distance along the wall normalised by the expansion length AB. In figure 5(*a*,*c*,*e*), these quantities are shown only for $s_w = 0.1$, 0.25 and 0.88. For $s_w = 0.05$, convergence was justifiably deduced from the baseline grid ($s_w = 0.1$) by showing similar separation characteristics. Based on these figures, we first note that there are no visible changes in surface parameters, starting from the medium grids towards finer grids. These grids also showed consistent flow features and an overall increase in the size of separation with grid refinement. Details near the corner (figure 5*b*,*f*), and near the leading edge (figure 5*d*), also show similar flow features in terms of the boundary layer length and resolution of corner eddies. Based on these observations, grids with n more than 1 million cells can be said to have achieved convergence. Interpretations of these flow features will be presented in the results and discussion section.

4.4. *Grid error analysis*

In the present study, the mixed-order method was used to carry out the grid error analysis. The method is considered appropriate for flows with discontinuities such as shock waves (Roy 2003). Starting with the series solution of the discretisation error,

$$f = f_{exact} + g_1 h + g_2 h^2 + O(h^3). \tag{4.1}$$

Here, f denotes the grid solution, h is the cell size, f_{exact} is the solution as $h \to 0$, the values of g are the order coefficients, and subscripts '1' and '2' are the orders of the error. Equation (4.1) requires that the solution to be within the asymptotic range and to contain no discontinuities. The mixed-order method, then, can be achieved by keeping the first- and second-order terms in (4.1), and expanding (4.1) for at least three grids. For an arbitrary mesh, f_{exact} can be obtained by using,

$$f_{exact} = f_1 + \frac{\epsilon_{32}(r_{12} - 1) - \epsilon_{21}(r_{12} r_{23}^2 - r_{12} - r_{23} - 1)}{(r_{12} - 1)(r_{23} - 1)(r_{12} r_{23} - 1)}, \tag{4.2}$$

where, $\epsilon_{32} = f_3 - f_2$, $\epsilon_{21} = f_2 - f_1$, $r_{12} = h_1/h_2$, $r_{23} = h_2/h_3$.

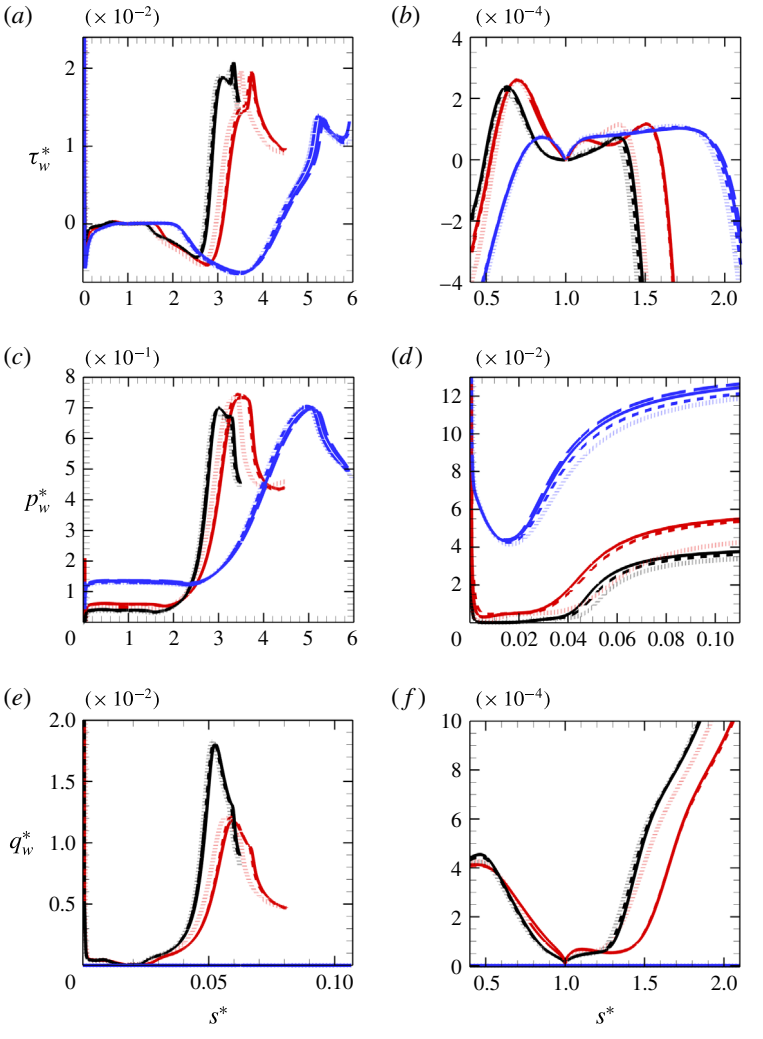

FIGURE 5. (Colour online) Convergence data for (*a*) global shear stress τ_w^*; (*b*) shear stress near the corner; (*c*) global surface pressure p_w^*; (*d*) pressure near the leading edge; (*e*) global heat flux q_w^*; (*f*) heat flux near the corner. Black line: $s_w = 0.1$; red line: $s_w = 0.25$; blue line: $s_w = 0.88$. Long-dashed line: grid 1; solid line: grid 2; dashed line: grid 3; dotted line: grid 4. (see table 2).

It is critical to point out that (4.2) is still an approximation, which is accurate to third order. f_{exact} is calculated at separation and reattachment to obtain the spatial error,

$$|\text{Spatial error}| = 3\left|\frac{f_{1-3} - f_{exact}}{f_{exact}}\right| \times 100, \tag{4.3}$$

noting that at separation, the expansion length L_e is more appropriate in the denominator of (4.3) to avoid any division near zero (Roy 2003). The factor '3' is a safety factor to obtain conservative estimate of the error. Table 3 shows the error values in per cent at separation (subscript '*S*') and reattachment (subscript '*R*'), and also at different wall temperatures. A systematic drop in the error with grid

	Index	%|Spatial error|$_S$	%|Spatial error|$_R$
	1	0.835	3.47
$s_w = 0.1$	2	1.47	5.75
	3	2.41	9.64
	1	0.050	0.72
$s_w = 0.25$	2	0.48	1.57
	3	3.63	14.31
	1	0.28	1.50
$s_w = 0.88$	2	00.43	3.61
	3	0.77	7.64
	4	1.37	8.29

TABLE 3. Spatial errors evaluated at separation and reattachment (see (4.3)).

refinement can be seen and indicate grid convergence. The spatial errors also seem to be maintained within 4 % and 15 % at separation and reattachment, respectively, for all grids. The results presented in § 4 are based on the fine grid solutions (Index 2).

5. Results and discussion

5.1. *Basic features of wall temperatures effects on laminar hypersonic leading edge separation*

Figures 6–8 show the shear stress, pressure and heat flux distributions, where the superscript '$*$' again denotes the values normalised by $0.5\rho_\infty U^2$ for the shear stress and pressure, and $0.5\rho_\infty U^3$ for the heat flux against the normalised distance $s^* = s/L_e$, where s is the wetted distance and L_e is the length of the expansion surface. The results are shown for the four temperature ratios under consideration (s_w of 0.05, 0.1, 0.25 and 0.88).

Considering the shear stress first, near the leading edge (figure 6*a*), separation (indicated by filled circles) is evidenced by the shear stress crossing the zero line (or changing sign), which occurs within a distance of less than 10 % from the leading edge, for all wall temperatures. We also note that separation is pushed upstream towards the leading edge as s_w is increased. The steep fall in shear stress prior to separation is due to the leading edge singularity. The open circles in figure 6(*a*) show locations of beginning of interaction, s_1^*. In the shear stress curve, the pressure rise appears to coincide with a 'knee' for $s_w = 0.05$–0.25 that becomes less obvious for the adiabatic wall, and the distance from the leading edge to s_1^* becomes less with increased wall temperature.

In figure 6(*b*), within the separated region, we see two minima in the shear stress distribution. The first minimum occurs soon after separation (closed circles), and the second is immediately followed by reattachment (open squares). The minimum before reattachment is found to be greater in magnitude than that after separation. The occurrence of two minima is typical of SBLI with large separated regions. Rizzetta *et al.* (1978), Bodonyi & Smith (1986), Elliott & Smith (1986), Smith (1988), Katzer (1989) and Smith & Khorrami (1991) have investigated this feature of SBLI in detail and attributed the second minimum to a reverse flow singularity/breakdown. Subsequently, Korolev *et al.* (2002) and Neiland *et al.* (2009) have shown that there need not be such a restriction (of a singularity) prior to reattachment in

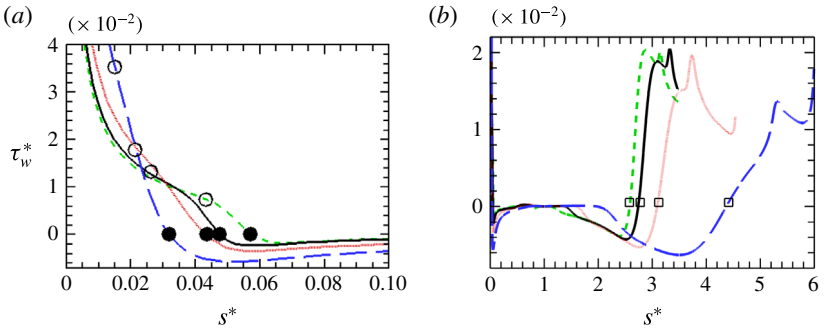

FIGURE 6. (Colour online) Wall temperature effect on shear stress: (*a*) close up near the leading edge and (*b*) global shear stress. Dashed green line: $s_w = 0.05$; solid black line: $s_w = 0.1$; dotted red line: $s_w = 0.25$; long-dashed blue line: $s_w = 0.88$. Closed circles: separation; open circles: beginning of interaction; squares: reattachment.

large-scale separations in terms of some critical scaled angle $\theta Re^{-1/4}$, where θ typically represents an incident shock or some other compressive disturbance such as a compression corner. Our results further showed that the flow transitions smoothly from separation to reattachment without any breakdown, and the second minimum becomes progressively shallower and more negative with increasing wall temperature (figure 6*b*).

Continuing with figure 6(*b*), after reattachment (indicated by open squares), we note that the shear stress reaches a maximum, and depending on the wall temperature, shows double peaks. This double peak is most prominent for the temperature ratios of 0.05 and 0.1. The first peak appears only slightly higher than the second at $s_w = 0.05$, whereas with $s_w = 0.1$, the second peak higher than the first. With moderate cooling at $s_w = 0.25$, the difference between the first and second peaks appear to be the greatest. Finally, in the adiabatic case (s_w = 0.88), the first peak is absent and only a single sharp peak is seen with a lower magnitude than the other wall temperatures. The first peak, when examined, coincides with the minimum neck area during recompression and the second peak with the triple point of separation and recompression shocks.

The presence of these peaks immediately following reattachment is due, firstly, to the formation of a neck (because of the sonic line being very close to the surface in the reattached boundary layer at high Mach numbers) preceding the intersection of separation and recompression shock system forming a triple point, also close to the surface springing an expansion fan leading to high shear stress. The double peak seems to be a feature of high Mach number hypersonic SBLI and this feature is confirmed at these flow conditions in the computations done by R. Hillier (Private communication, 2015) using a different numerical code.

Figure 7 shows the corresponding surface pressure near the leading edge (*a*) and global surface pressure (*b*). Near the leading edge, the pressures, on reaching a minimum soon after the leading edge, show a sudden rise towards separation in which its slope rises with rising wall temperature. Further, the boundary layer extent prior to separation can be determined from the distance from the leading edge to the beginning of interaction. In the case of the coldest wall considered, $s_w = 0.05$, the boundary layer reaches 8 % of the distance from the leading edge and reduces to nearly 4 % for the adiabatic wall. These results are consistent with the findings of Khorrami & Smith (1994), who showed that the upstream influence

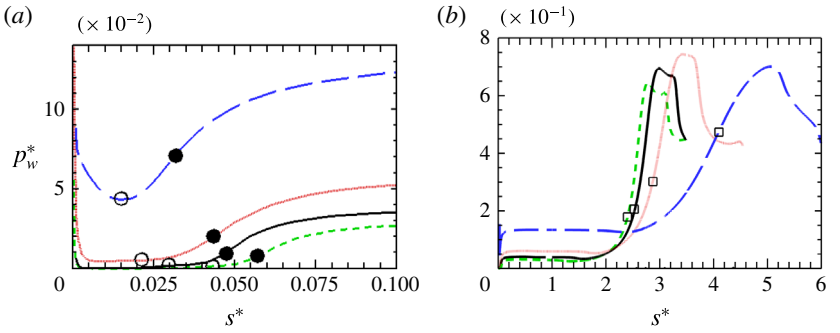

FIGURE 7. (Colour online) Wall temperature effect on surface pressure: (*a*) close-up near the leading edge and (*b*) global surface pressure. Dashed green line: $s_w = 0.05$; solid black line: $s_w = 0.1$; dotted red line: $s_w = 0.25$; long-dashed blue line: $s_w = 0.88$. Closed circles: separation; open circles: beginning of interaction; squares: reattachment.

distance for hypersonic flow over a semi-infinite flat plate is reduced by both a higher wall temperature and lower viscous interaction parameter (defined as $M/Re^{1/6}$). They looked at various wall temperatures and cases where the viscous interaction parameter, as per their definition, is equal to or greater than 2. The viscous interaction parameter calculated for the present wall temperatures varies between 2.6 for s_w 0.05, and 3 for the s_w 0.88. Here, the effect of increasing wall temperature, in reducing the upstream influence distance, appears to outweigh the effect of viscous interaction parameter. The greater drop in pressure with wall temperature is also in accordance with Khorrami and Smith's (1994) findings. Neiland *et al.* (2009) and Shvedchenko (2009) have further noted that the leading edge has no critical effect on the solution downstream and disturbances dissipate quite rapidly with distance downstream. After separation, the pressures reach a plateau that spans over the whole expansion surface. With the increase in wall temperature, we see that the magnitude of the plateau and length of the separated region are increased. Compared to the length of the separated region (the straight distance between *S* and *R*) of the adiabatic wall, the separation length at the lower wall temperatures, $s_w = 0.25$, 0.1 and 0.05 is reduced by 32 %, 39.5 % and 43.5 %, respectively. These features are consistent with those found by Neiland *et al.* (2009).

Examination of pressure distributions in figure 7(*b*) further reveals additional features. For instance, prior to reattachment, the pressure shows a perceptible decrease from the plateau value before rising again. This 'dip' in the plateau pressure is indicative of a secondary separation near the corner. This has been noted and commented upon previously by Smith & Khorrami (1991) and more recently by Korolev *et al.* (2002). Shvedchenko (2009) has also noted that while this dip in pressure is sharp and rapid at high Reynolds numbers, there is a 'smearing' effect at lower Reynolds numbers. In the present instance, the Reynolds numbers are of the order of 1×10^3 so that these features are spread out and diffused. Another aspect is that in post-reattachment the pressures show similar double peaks as in the shear stress distribution, in which the first is associated with the neck region and second with the triple point of the separation and reattachment shocks along with an emanating expansion wave and a slip line. The intersection of separation and reattachment shocks accompanied by an expansion and a slip line is usually referred to as Edney type VI shock/shock interference (Edney 1968).

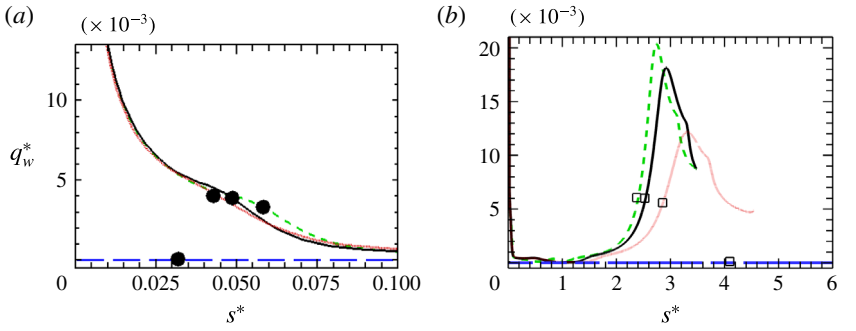

FIGURE 8. (Colour online) Wall temperature effect on heat flux: (*a*) close-up near the leading edge and (*b*) global heat flux. Dashed green line: $s_w = 0.05$; solid black line: $s_w = 0.1$; dotted red line: $s_w = 0.25$; long-dashed blue line: $s_w = 0.88$. Closed circles: separation; open circles: beginning of interaction; squares: reattachment.

Effects of wall temperature on overall heat flux in (*b*) and in the vicinity of the leading edge (*a*) are shown in figure 8. We observe that with decreasing wall temperature, the heat flux increases as expected and is zero for the adiabatic case. The maximum heat flux is seen in figure 8(*b*) as a single sharp peak with no obvious second peak, as in shear stress and pressure, although at $s_w = 0.25$, there is a hint of a 'knee' shortly after the peak. The decrease in peak heat flux with increase in wall temperature seems to be a strongly nonlinear function of wall temperature. With increase in s_w from 0.05 to 0.1, it decreases by 7.5 % but at s_w at 0.25, it has decreased by approximately 40 %. A 'knee' also appears for s_w 0.05 and 0.1 at separation (closed circles in figure 8*a*). The beginning of interaction is less distinguishable for the heat flux and is thus not shown.

Lastly, figure 9 shows the effect of wall temperature, expressed in terms of s_w, on the locations of separation and reattachment (figure 9*a*), separation, reattachment and plateau pressures (figure 9*b*) and peak heat flux, $q^*_{w,max}$ (figure 9*c*). It is important to note that in order to show these figures on the same scale, we have lowered the order of the reattachment values (location and pressure) by a factor of 10 whilst the others remain unchanged. This exercise is interesting because, due to a dominant nonlinear behaviour, two distinct regions of wall temperature are apparent. First, for $s_w < 0.25$, the effect of wall cooling is greater on separation, and to a lesser degree on the reattachment pressure. And second, for $s_w > 0.25$, these features drop towards the adiabatic value, while the reattachment pressure increases towards the adiabatic value. These features seem to indicate the wall temperature effects are greater on reattachment, plateau pressure and maximum heat flux than on separation.

5.2. *Flow near the corner*

Figure 10(*a*) shows the shear stress distribution in the vicinity of the corner between $0.4 \leqslant s^* \leqslant 2.1$. The corresponding heat flux and pressure are shown in figure 10(*b*,*c*). We note that the shear stress crosses zero, becoming positive, then goes to zero at the vertex after reaching a peak. This is true for all wall temperature studied here. The shear stress then becomes positive again only to reach another peak before becoming negative. This double loop within the main separation bubble is due to the discontinuity at the vertex, where the shear stress must go to zero. The double loop

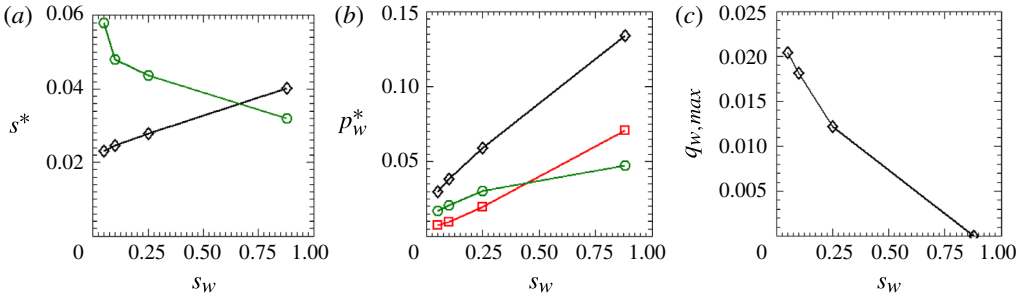

FIGURE 9. (Colour online) Effects of s_w on (*a*) onset of separation (green circles) and reattachment (black diamonds), (*b*) pressure at separation (red squares); pressure plateau (black diamonds); reattachment (green circles) and (*c*) peak heat flux, $q^*_{w,max}$.

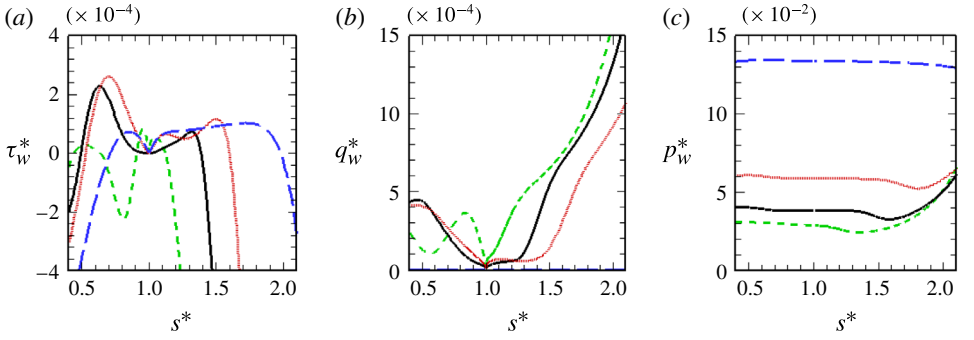

FIGURE 10. (Colour online) Flow near the corner: (*a*) shear stress, (*b*) heat flux and (*c*) pressure. Dashed green line: $s_w = 0.05$; solid black line: $s_w = 0.1$; dotted red line: $s_w = 0.25$; long-dashed blue line: $s_w = 0.88$.

is a manifestation of a secondary corner eddy. The shape and size of this eddy seems to be dependent on the wall temperature.

At $s_w = 0.05$, the corner eddy is small (and slightly asymmetric) with respect to the vertex. A feature to note here is the emergence of a small third eddy in the region $0.4 \leqslant s^* \leqslant 0.6$. At $s_w = 0.1$ there is a single corner eddy, which has grown to a length nearly half that of the expansion surface, and crosses the corner towards the compression surface. The small third eddy seen at $s_w = 0.05$, however, seems to have been swallowed by the larger corner eddy. This is due to the interaction between diffusion and convection of vorticity resulting in stretching of filaments of vorticity at the corner, and the smaller eddy (Burggraf 1966). The main vortex has moved downstream with its centre towards the compression surface. At $s_w = 0.25$, we again notice other significant changes: first, the corner eddy has grown much bigger with its centre now almost symmetrically disposed with respect to the vertex, and the main vortex meanwhile has shifted downstream being stretched further. With the adiabatic wall ($s_w = 0.88$), both the main vortex and the corner eddy are both stretched and located predominantly on the compression side.

It seems clear that both the size and shape of the corner and the main vortex are strongly dependent on the wall temperature and there seems to be a shift downstream with increase in wall temperature. As pointed out by Burggraf (1966), the dependence of vorticity and its distribution in the recirculating region seems clearly related to the thermal energy distribution.

Presence of multiple eddies embedded within the main vortex, in a large separated flow, has been noted previously in numerical studies by Neiland *et al.* (2009) and Shvedchenko (2009) on ramp-induced separations at large angles (10°–20°). Shvedchenko (2009) identifies a scaled ramp angle as the critical parameter for the occurrence of these multiple vortices independent of the wall temperature. This scaled ramp angle ξ_o is defined as $\theta Re^{1/4}$, where θ is the geometric angle. Neiland *et al.* (2009) and Shvedchenko (2009) show that separation size and occurrence of multiple vortices is a strong function of both ξ_o and s_w, and that with increase of both, the separation is pushed upstream towards the leading edge of the plate and the reattachment downstream on the ramp. For angles $\theta \geqslant 20°$, separation occurs at the leading edge. Shvedchenko (2009) delineates various separation stages based on the value of ξ_o with the wall temperature having a small or no effect. For example, for small steady separation at the ramp corner, $2 \leqslant \xi_o \leqslant 3$ for cooled and adiabatic walls alike. For steady secondary separation, $5 \leqslant \xi_o \leqslant 6$ with no effect of the wall temperature. When $\xi_o \leqslant 7$, Shvedchenko (2009) shows that instability arises in secondary separation giving way to multiple small-scale eddies, and the secondary separation becomes completely unsteady for $\xi_o \geqslant 10$. It should be pointed out here that ξ_o as defined by Shvedchenko (2009) is slightly different from that of Rizzetta (1976), who define the scaled corner angle α in terms of the triple-deck scales,

$$\alpha = \frac{\alpha^* Re^{1/4}}{C^{1/4}\lambda^{1/2}M_e^{1/2}}, \tag{5.1}$$

which includes the effects of viscosity C, wall shear λ and the Mach number M_e at the edge of the boundary layer taking into account all components of the interaction. α^* is the geometric angle in their notation.

A similar expression has been used by Korolev *et al.* (2002) to identify primary and secondary vortices. They define it as a controlling similarity parameter for the ramp-induced SBLI. According to this criterion, secondary separation occurs when $\alpha \approx 5$. Our data, based on C and λ evaluated for the various wall temperatures, show that the secondary eddy appears in the range of α 3–6, the higher value signifying the lowest wall temperature and the lower value the adiabatic wall temperature thereby showing a somewhat higher effect of the wall temperature.

The heat flux distribution near the corner is shown in figure 10(*b*). As expected, q_w^* goes to zero at the corner vertex and decreases with s_w until it reaches zero for the adiabatic wall. The heat flux distribution for $s_w = 0.05$ shows the maximum variation, and the presence of the corner eddy has the effect of reducing q_w^* for the isothermal walls. The latter is evidenced by the sudden drop near $s^* = 0.4$ for $s_w = 0.1$ and $s_w = 0.25$, and soon after the nascent eddy ($s_w^* = 0.75$) at $s_w = 0.05$. The heat flux also appears to be a mirror image of the shear stress (excluding the adiabatic wall), in the sense that an increase in shear stress is associated with a decrease in the heat flux, and the maxima in shear stress are seen as minima in the heat flux (and *vice versa*). Figure 10(*c*), similarly, shows the pressure distribution in the corner region. Though the pressure appears largely constant for all values of s_w, we observe a slight drop near the corner. This drop is reduced with the increase in s_w, and reaches a maximum (6.5 %) for $s_w = 0.05$. Downstream, we notice an inflection point coinciding with the onset of the corner eddy, and at $s^* = 1.35$, 1.6 and 1.75 for $s_w = 0.05$, 0.1 and 0.25 (not seen in the adiabatic wall), the dip indicating the beginning of the recompression process and the neck region is clearly seen. Essentially, this shows that as the wall temperature increases, the recompression process is delayed and as

a result, these corner eddies are dragged downstream onto the compression surface. Neiland *et al.* (2009) relates the movement of reattachment to the centre of pressure hence the static stability. Nieland and his associates showed that for such a case of large separation, as the centre of pressure as seen by the stretching of pressure plateau towards the compression surface, the static stability improves, as opposed to small separations where it worsens.

Evolution of the corner eddy and displacement of vortices with changing wall temperature ratio can be seen in figure 11. Here, the streamline patterns superimposed on temperature contours are shown. We see that, while the outer flow is mainly dominated by low temperature, as the wall temperature is increased, the temperature gradients are relieved within the recirculating region with the tertiary eddy at $s_w = 0.05$ possibly amalgamated with the corner eddy.

Presence of secondary eddies have been previously noted and studied at low speeds (Burggraf 1966; Higdon 1985), supersonic (Mohri & Hillier 2011; Sridhar, Gai & Kleine 2016), and hypersonic Mach numbers (Jackson, Hillier & Soltani 2001) in convergent channels and rectangular cavities. Moffatt (1964) has explained the existence of such eddies as due to the effects of viscosity and low local velocities at the corner. The theoretical reasoning given by Moffatt is that, provided the included angle of the corner is less than 146°, an infinite number of eddies can exist. However, because of dissipative effect of viscosity, their number and intensity decrease rapidly in geometric progression as the corner is approached so that, in effect, a single stable eddy may exist. In their study of step-induced separation in hypersonic low density flow, Leite & Santos (2015) attributed the existence of a secondary corner eddy to a Moffatt-type eddy. In the present instance, as the included angle is within the limits set by Moffatt, such a possibility cannot be excluded.

The reason advanced by Neiland *et al.* (2009) for the existence of multiple vortices in large separated flows (their maximum included angle is 160°) and with increasing wall temperature is that, as a result of separation of the reverse flow boundary layer (Burggraf 1973; Stewartson & Williams 1973; Burggraf 1975; Rizzetta 1976), the normal pressure gradient is no longer negligible in the separated region. To examine this aspect, figure 12(*a–c*) shows the pressure variation normalised here with respect p_∞ at three locations: beginning of interaction, at the corner and in the reattachment region, respectively. n^* denotes the normal distance to the wall.

We first note that variations in the pressure normal to the surface n^* become more significant with increasing wall temperature, particularly at the beginning of the interaction and at reattachment. This holds valid at the three locations examined. As the boundary layer separates near the leading edge, pressure gradients (figure 12*a*) exist and are maximum for the adiabatic wall (earlier separation) and minimum for $s_w^* = 0.05$ (approaching the Blasius boundary layer). In figure 12(*b*), on the other hand, the pressure variations in the corner region indicate visible differences, but much less in comparison to those at the beginning of the interaction. With the steady corner eddy with an adiabatic wall, the normal pressure (thus gradient), do not seem to vary much until the flow reaches the dividing streamline. In the reattachment region, figure 12(*c*), the pressure gradient $\mathrm{d}p/\mathrm{d}n$ is again significant, as expected.

The corresponding temperature profiles are shown in figure 13(*a–c*). The temperature, T, is normalised with respect to the free-stream value and n^* is again the normal distance from the wall. Similar observations in the temperature gradient $\mathrm{d}T/\mathrm{d}n$ are seen as in the pressure gradient, except that in the separation region (figure 13*b*), the temperature gradients are more pronounced. Comparison of these profiles at various wall temperatures also gives an indication to the nonlinear behaviour of heat flux as discussed earlier with reference to figure 9(*c*).

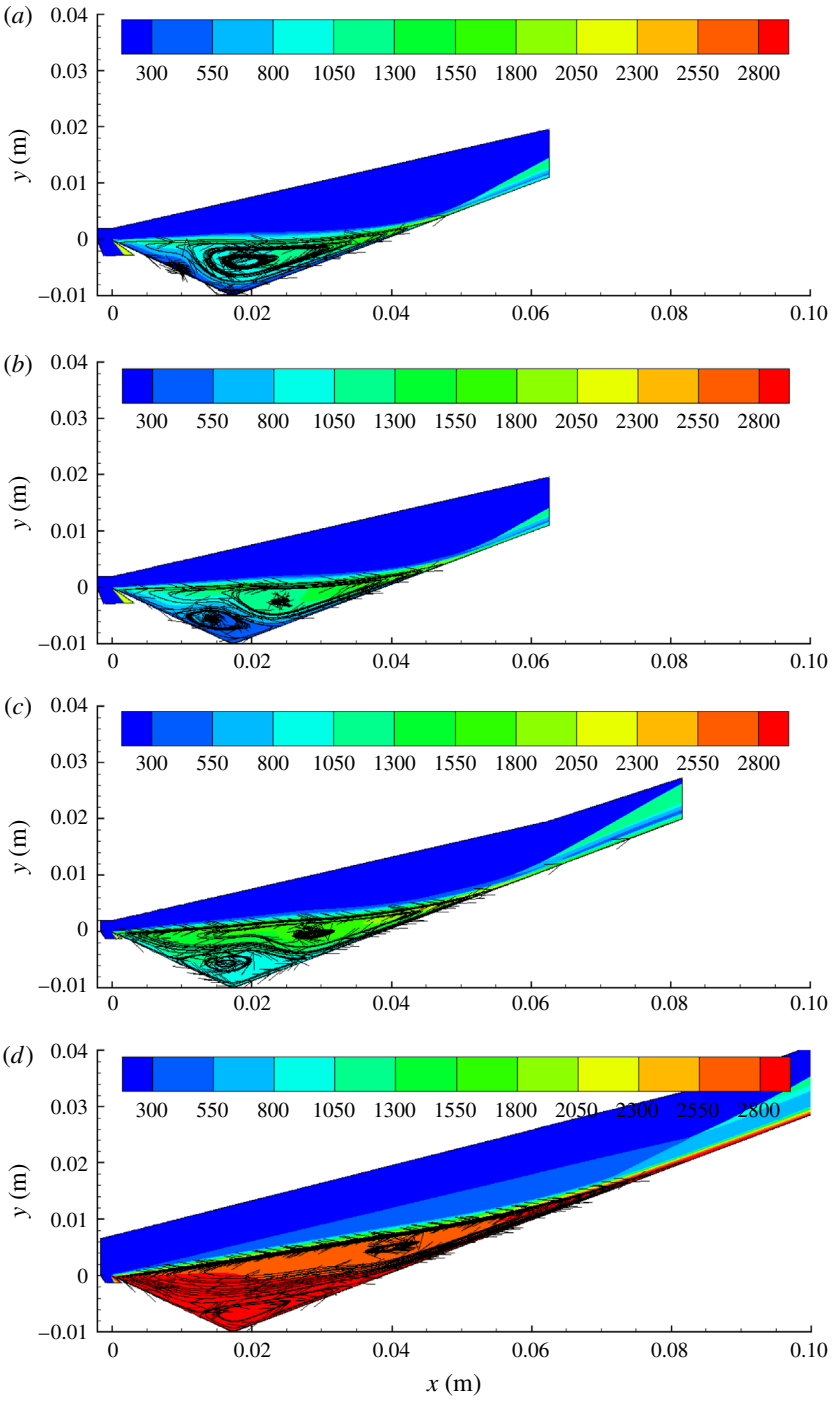

FIGURE 11. Streamlines and temperature contours (in K) show the effect of temperature distribution on the evolution of corner eddies. (*a*) $s_w = 0.05$, (*b*) $s_w = 0.1$, (*c*) $s_w = 0.25$, (*d*) $s_w = 0.88$.

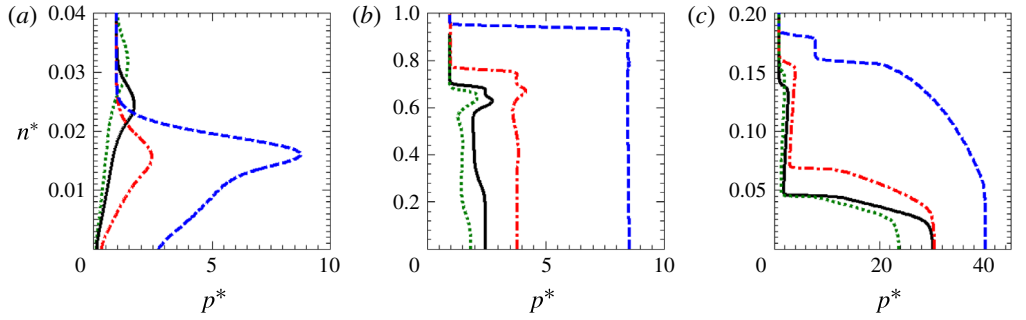

FIGURE 12. (Colour online) Normal pressure distribution at various locations: (*a*) at the beginning of interaction; (*b*) near the corner; (*c*) near reattachment. p^* is normalised by the free-stream pressure. Dotted green line: $s_w = 0.05$; black solid line: $s_w = 0.1$; dash-dotted red line: $s_w = 0.25$; dashed blue line: $s_w = 0.88$.

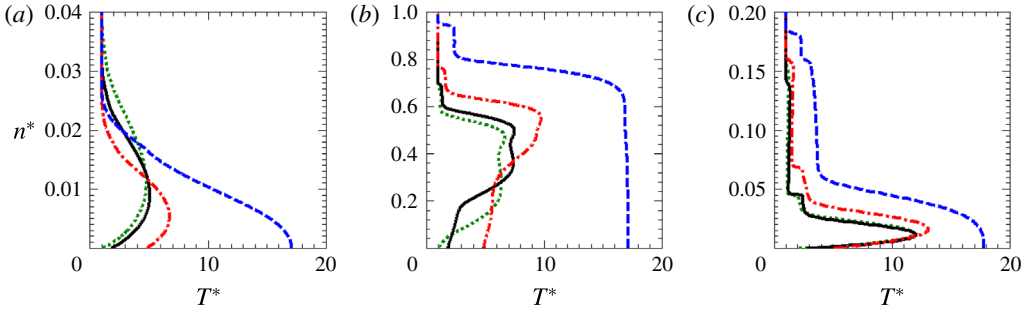

FIGURE 13. (Colour online) Normal temperature distribution at various locations: (*a*) at the beginning of interaction; (*b*) near the corner; (*c*) near reattachment. p^* is normalised by the free stream. Dotted green line: $s_w = 0.05$; black solid line:$s_w = 0.1$; dash-dotted red line: $s_w = 0.25$; dashed blue line: $s_w = 0.88$.

5.3. *Interpretation in terms of triple-deck scales*

Having established the basic characteristics of laminar hypersonic leading edge separation under cold and adiabatic wall conditions, it is tempting to seek to express all the data in terms of the universal curve as discussed in Lewis, Kubota & Lees (1968) and Stewartson & Williams (1969). However, it turned out to be not very meaningful as the boundary layer before separation seen in the present case is not a fully developed boundary as assumed in standard triple-deck problems. In terms of Stewartson and Williams scales, we have,

$$X = \left(\frac{s - s_c}{s_c}\right)\left[\left(\frac{M_\infty^{1/4}}{\epsilon}\right)^2 \lambda^{5/4} C^{-3/8}\right]\left(\frac{T_w}{T_\infty}\right)^{3/2}, \tag{5.2}$$

and,

$$P = \left(\frac{p - p_\infty}{p_\infty}\right)\left[\left(\frac{M_\infty^{1/4}}{\epsilon}\right)^2 \frac{\lambda^{-1/2} C^{-1/4}}{\gamma M_\infty^2}\right]. \tag{5.3}$$

For given free-stream conditions, wall temperatures and an unperturbed fully developed boundary layer, all the parameters inside the square brackets in (5.2)

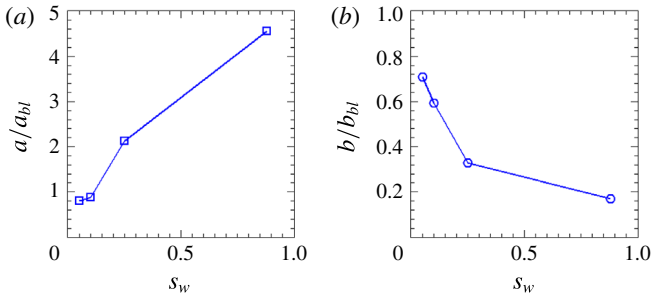

FIGURE 14. (Colour online) Deviation of the present data from the Blasius boundary layer in the triple-deck theory; (*a*,*b*) take into account the effects of varying flow conditions at the edge of the boundary layer with wall temperature as opposed to the standard triple-deck formulation.

and (5.3) become constants so that the triple-deck theory suggests a universal curve seen in previous SBLI studies, and also shown to be experimentally valid by Lewis *et al.* (1968). However, in the presence of a leading edge separation, the boundary layer is growing under an adverse pressure gradient so that the Mach number, ϵ and λ are no longer constants, and even C was seen to be varying slightly depending on the wall temperature. As noted earlier, separation pressures seem no longer independent of wall temperatures as has been the case of interactions with well-developed boundary layers prior to separation.

The discrepancy in the scales of X and P between the present case and the SBLI with a prior well-developed boundary layer is illustrated in figure 14. a/a_{bl} represents the present values in the square brackets in (5.2) normalised by M_∞, $Re_{\infty,Le}$, λ and C. Similarly, the parameter b/b_{bl} represents the deviation of P from the Blasius values. We immediately see that, firstly, the discrepancy in the X scaling is much more than that of P, as expected. We see that with moderate to no cooling (adiabatic), the discrepancy increases by more than a factor of 2 in the case of X. On the other hand, with the two coldest wall cases (where the boundary layer growth is considerably larger), the deviation is much less in the case of both X and P. Another point to note is that the deviation in P from the coldest to adiabatic wall is increased by nearly 80 %.

6. Summary and conclusions

Hypersonic leading edge separation along with effects of wall temperature on separation have been studied numerically. Such a geometry was first used by Chapman *et al.* (1958) to propose their isentropic recompression theory, which is shown to be generally valid at high Reynolds numbers and low Mach numbers with no pre-existing boundary layer. The present hypersonic results show that due to strong viscous effects, separation occurs not at the leading edge but slightly downstream of it (within 10 % of the distance from the leading edge) and shown to have strong dependence on wall temperature. The higher the wall temperature, the closer was the separation location to the leading edge. In all cases, however, there was a discernible growth of the boundary layer before interaction and separation. In the range of wall temperatures studied, the flow was mainly in the subcritical range (large Neiland number) and only in the case of adiabatic wall it was seen to be nearly transcritical (Neiland number of the order unity).

The existence of multiple vortices embedded in large separated flows, as previously seen in the investigations of Neiland and his co-researchers, has been verified. In the present investigation, the separated flow was found to consist of a main vortex and an embedded corner eddy. For colder wall temperatures, both the main vortex and the corner eddy were predominantly disposed towards the expansion surface. They migrated downstream towards the compression surface with increase in wall temperature. Another feature of the corner eddy found in this investigation was its double-loop nature which is attributed to the discontinuity at the vertex.

Although the hypersonic leading edge separation showed many features of free interaction, there were significant differences due to strong effect of the leading edge which inhibits the Blasius-type constant pressure boundary layer before interaction. These differences are accentuated with increase in wall temperature causing separation to move upstream towards the leading edge. These are highlighted and discussed. The study has clearly shown the need for more numerical studies as well as benchmark experimental data.

Acknowledgements

The authors are grateful to the Australian research Council for their support under grant (DP-140100842). They would also like to acknowledge National Facility Systems (NCI) for computer resources, and the US Office of Aerospace Research and Development (AOARD) for their support. Finally but by no means least, our sincere thanks are due to Professor G. Candler, of the University of Minnesota, for permission to use his US3D code for this investigation. We would like to thank the referees for their helpful comments and criticism, which have helped improve the paper.

REFERENCES

BLOTTNER, F. G., JOHNSON, M. & ELLIS, M. 1971 Chemically reacting viscous flow program for multi-component gas mixtures. *Tech. Rep.* Sandia Labs., Albuquerque, N. Mex.

BODONYI, R. J. & SMITH, F. T. 1986 Shock-wave laminar boundary-layer interaction in supercritical transonic flow. *Comput. Fluids* **14** (2), 97–108.

BROWN, S. N., CHENG, H. K. & LEE, C. J. 1990 Inviscid–viscous interaction on triple-deck scales in a hypersonic flow with strong wall cooling. *J. Fluid Mech.* **220**, 309–337.

BROWN, S. N. & STEWARTSON, K. 1969 Laminar separation. *Annu. Rev. Fluid Mech.* **1** (1), 45–72.

BROWN, S. N., STEWARTSON, K. & WILLIAMS, P. G. 1975 Hypersonic self-induced separation. *Phys. Fluids* **18** (6), 633–639.

BURGGRAF, O. R. 1966 Analytical and numerical studies of the structure of steady separated flows. *J. Fluid Mech.* **24** (01), 113–151.

BURGGRAF, O. R. 1973 Inviscid reattachment of a separated shear layer. In *Proceedings of the 3rd International Conference on Numerical Methods in Fluid Mechanics*, pp. 39–47. Springer.

BURGGRAF, O. R. 1975 Asymptotic theory of separation and reattachment of a laminar boundary layer on a compression ramp. *Tech. Rep.* DTIC Document.

BURGGRAF, O. R., RIZZETTA, D., WERLE, M. J. & VATSA, V. N. 1979 Effect of Reynolds number on laminar separation of a supersonic stream. *AIAA J.* **17** (4), 336–343.

CANDLER, G. V., JOHNSON, H. B., NOMPELIS, I., GIDZAK, V. M., SUBBAREDDY, P. K. & BARNHARDT, M. 2015 Development of the US3D code for advanced compressible and reacting flow simulations. In *53rd AIAA Aerospace Sciences Meeting*, p. 1893.

CANDLER, G. V., SUBBAREDDY, P. K. & BROCK, J. M. 2014 Advances in computational fluid dynamics methods for hypersonic flows. *J. Spacecr. Rockets* **52** (1), 17–28.

CASSEL, K. W., RUBAN, A. I. & WALKER, J. A. 1995 An instability in supersonic boundary-layer flow over a compression ramp. *J. Fluid Mech.* **300**, 265–285.

CASSEL, K. W., RUBAN, A. I. & WALKER, J. D. A. 1996 The influence of wall cooling on hypersonic boundary-layer separation and stability. *J. Fluid Mech.* **321**, 189–216.

CHAPMAN, D. R., KUEHN, D. M. & LARSON, H. K. 1958 Investigation of separated flows in supersonic and subsonic streams with emphasis on the effect of transition. *NACA Tech. Rep.* 1356.

CHENG, H. K. 1993 Perspectives on hypersonic viscous flow research. *Annu. Rev. Fluid Mech.* **25** (1), 455–484.

DRAYNA, T. W., NOMPELIS, I. & CANDLER, G. V. 2006 Numerical simulation of the aedc waverider at mach 8. *AIAA Paper* 2816.

EDNEY, B. E. 1968 Effects of shock impingement on the heat transfer around blunt bodies. *AIAA J.* **6** (1), 15–21.

ELLIOTT, J. W. & SMITH, F. T. 1986 Separated supersonic flow past a trailing edge at incidence. *Comput. Fluids* **14** (2), 109–116.

GADD, G. E. 1957 An experimental investigation of heat transfer effects on boundary layer separation in supersonic flow. *J. Fluid Mech.* **2** (02), 105–122.

GAJJAR, J. & SMITH, F. T. 1983 On hypersonic self-induced separation, hydraulic jumps and boundary layers with algebraic growth. *Mathematika* **30** (1), 77–93.

HAYES, W. D. & PROBSTEIN, R. F. 1959 *Hypersonic Flow Theory*. Elsevier.

HIGDON, J. L. 1985 Stokes flow in arbitrary two-dimensional domains: shear flow over ridges and cavities. *J. Fluid Mech.* **159**, 195–226.

HOLDEN, M. S., WADHAMS, T. P., MACLEAN, M. G. & DUFRENE, A. T. 2013 Measurements of real gas effects on regions of laminar shock wave/boundary layer interaction in hypervelocity flows for blindcode validation studies. *Air Force Office of Scientific Research Rep.* AFRL-OSR-VA-TR-2013-0134. Virginia, USA.

JACKSON, A. P., HILLIER, R. & SOLTANI, S. 2001 Experimental and computational study of laminar cavity flows at hypersonic speeds. *J. Fluid Mech.* **427**, 329–358.

KATZER, E. 1989 On the lengthscales of laminar shock/boundary-layer interaction. *J. Fluid Mech.* **206**, 477–496.

KERIMBEKOV, R. M., RUBAN, A. I. & WALKER, J. D. A. 1994 Hypersonic boundary-layer separation on a cold wall. *J. Fluid Mech.* **274**, 163–195.

KHORRAMI, A. F. & SMITH, F. T. 1994 Hypersonic aerodynamics on thin bodies with interaction and upstream influence. *J. Fluid Mech.* **277**, 85–108.

KOROLEV, G. L., GAJJAR, J. B. & RUBAN, A. I. 2002 Once again on the supersonic flow separation near a corner. *J. Fluid Mech.* **463**, 173–199.

LEITE, P. H. M. & SANTOS, W. F. N. 2015 Computational analysis of the flow field structure of a non-reacting hypersonic flow over forward-facing steps. *J. Fluid Mech.* **763**, 460–499.

LEWIS, J. E., KUBOTA, T. & LEES, L. 1968 Experimental investigation of supersonic laminar, two-dimensional boundary-layer separation in a compression corner with and without cooling. *AIAA J.* **6** (1), 7–14.

LIGHTHILL, M. J. 1953 On boundary layers and upstream influence. II. Supersonic flows without separation. *Proc. R. Soc. Lond.* A **217** (1131), 478–507.

MESSITER, A. F. 1970 Boundary-layer flow near the trailing edge of a flat plate. *SIAM J. Appl. Maths* **18** (1), 241–257.

MILLIKAN, R. C. & WHITE, D. R. 1963 Systematics of vibrational relaxation. *J. Chem. Phys.* **39** (12), 3209–3213.

MOFFATT, H. K. 1964 Viscous and resistive eddies near a sharp corner. *J. Fluid Mech.* **18** (01), 1–18.

MOHRI, K. & HILLIER, R. 2011 Computational and experimental study of supersonic flow over axisymmetric cavities. *Shock Waves* **21** (3), 175–191.

NEILAND, V. Y. 1969 Theory of laminar boundary layer separation in supersonic flow. *Fluid Dyn.* **4** (4), 33–35.

NEILAND, V. Y. 1970 Asymptotic theory of plane steady supersonic flows with separation zones. *Fluid Dyn.* **5** (3), 372–381.

NEILAND, V. Y. 1973 Boundary-layer separation on a cooled body and its interaction with a hypersonic flow. *Fluid Dyn.* **8** (6), 931–939.

NEILAND, V. Y., BOGLEPOV, V. V., DUDIN, G. N. & LIPATOV, I. 2008 *Asymptotic Theory of Supersonic Viscous Gas Flows*. Butterworth-Heinemann.

NEILAND, V. Y., SOKOLOV, L. A. & SHVEDCHENKO, V. V. 2009 Temperature factor effect on separated flow features in supersonic gas flow. In *BAIL 2008-Boundary and Interior Layers*, pp. 39–54. Springer.

NOMPELIS, I. & CANDLER, G. V. 2014 US3D predictions of double-cone and hollow cylinder-flare flows at high enthalpy. In *44th AIAA Fluid Dynamics Conference*.

PARK, C. 1993 Review of chemical-kinetic problems of future nasa missions in earth entries. *J. Thermophys. Heat Transfer* **7** (3), 385–398.

PARK, G., GAI, S. L. & NEELY, A. J. 2010 Laminar near wake of a circular cylinder at hypersonic speeds. *AIAA J.* **48** (1), 236–248.

RIZZETTA, D. P. 1976 Asymptotic solution for two-dimensional viscous supersonic and hypersonic flows past compression and expansion corners. PhD thesis, Ohio State University.

RIZZETTA, D. P., BURGGRAF, O. R. & JENSON, R. 1978 Triple-deck solutions for viscous supersonic and hypersonic flow past corners. *J. Fluid Mech.* **89** (03), 535–552.

ROY, C. J. 2003 Grid convergence error analysis for mixed-order numerical schemes. *AIAA J.* **41** (4), 595–604.

SEDDOUGUI, S. O., BOWLES, R. I & SMITH, F. T. 1991 Surface-cooling effects on compressible boundary-layer instability. *Eur. J. Mech. (*B*/Fluids)* **10** (2), 117–145.

SHVEDCHENKO, V. V. 2009 About the secondary separation at supersonic flow over a compression ramp. *TsAGI Sci. J.* **40** (5), 587–607.

SMITH, F. T. 1986 Steady and unsteady boundary-layer separation. *Annu. Rev. Fluid Mech.* **18** (1), 197–220.

SMITH, F. T. 1988 A reversed flow dingularity in interacting boundary layers. *Proc. R. Soc. Lond.* A **420** (1858), 21–52.

SMITH, F. T. & KHORRAMI, A. F. 1991 The interactive breakdown in supersonic ramp flow. *J. Fluid Mech.* **224**, 197–215.

SRIDHAR, V., GAI, S. L. & KLEINE, H. 2016 Oscillatory characteristics of shallow open cavities in supersonic flow. *AIAA J.* **54** (11), 3495–3508.

STEWARTSON, K. 1964 *The Theory of Laminar Boundary Layers in Compressible Fluids,* vol. 3. Cambridge University Press.

STEWARTSON, K. 1974 Multistructured boundary layers on flat plates and related bodies. *Adv. Appl. Mech.* **14**, 145–239.

STEWARTSON, K. 1975 On the asymptotic theory of separated and unseparated fluid motions. *SIAM J. Appl. Maths* **28** (2), 501–518.

STEWARTSON, K. & WILLIAMS, P. G. 1969 Self-induced separation. *Proc. R. Soc. Lond.* A **312** (1509), 181–206.

STEWARTSON, K. & WILLIAMS, P. G. 1973 On self-induced separation II. *Mathematika* **20** (01), 98–108.

SYCHEV, V. V., RUBAN, A. I., SYCHEV, V. V. & KOROLEV, G. L. 1998 *Asymptotic Theory of Separated Flows*. Cambridge University Press.

VAN LEER, B. 1979 Towards the ultimate conservative difference scheme. V. A second-order sequel to Godunov's method. *J. Comput. Phys.* **32** (1), 101–136.

WILKE, C. R. 1950 A viscosity equation for gas mixtures. *J. Chem. Phys.* **18** (4), 517–519.

WRIGHT, M. J., CANDLER, G. V. & BOSE, D. 1998 Data parallel line relaxation method for the Navier–Stokes equations. *AIAA J.* **36** (9), 1603–1609.